

1 Identifying plausible historical scenarios for coupled lake level  
2 and seismicity rate changes: The case for the Dead Sea during  
3 the last two millennia.

4 **Mariana Belferman<sup>1</sup>, Amotz Agnon<sup>2</sup>, Regina Katsman<sup>1</sup> and Zvi Ben-Avraham<sup>1</sup>**

5 <sup>1</sup> *The Dr. Moses Strauss Department of Marine Geosciences, Leon H. Charney School of Marine  
6 Sciences, University of Haifa, Mt. Carmel, Haifa 3498838, Israel.*

7 <sup>2</sup> *The Fredy & Nadine Herrmann Institute of Earth Sciences, The Hebrew University of  
8 Jerusalem, Jerusalem 9190401, Israel*

9 Mariana Belferman: [mkukuliev@gmail.com](mailto:mkukuliev@gmail.com) (corresponding author)

10 Amotz Agnon: [amotz@huji.ac.il](mailto:amotz@huji.ac.il)

11 Regina Katsman: [rkatsman@univ.haifa.ac.il](mailto:rkatsman@univ.haifa.ac.il)

12 Zvi Ben-Avraham: [zviba@post.tau.ac.il](mailto:zviba@post.tau.ac.il)

### 13 **ABSTRACT**

14 Seismicity triggered by water level changes in reservoirs and lakes is usually studied from well-

15 documented contemporary records. Can such triggering be explored on a historical time scale

16 when the data gathered on water level fluctuations in historic lakes and the earthquake catalogs

17 suffer from severe uncertainties? These uncertainties stem from the different nature of the data

18 gathered, methods, and their resolution. In this article, we show a way to considerably improve

19 the correlation between interpolated records of historical<sup>1</sup> water level reconstructions at the Dead

20 Sea and discrete seismicity patterns in the area<sup>2</sup>, over the period of the past two millennia.

21 Inspired by the results of our previous study, we carefully revise the historical earthquake catalog

22 in the Dead Sea keeping only events with documented destruction in Jerusalem, the largest  
23 historical city in the vicinity of the lake. We then generate an ensemble of random interpolations  
24 of water level curves and rank them by correlation with the historical records of seismic stress  
25 release. We numerically simulate a synthetic catalog of earthquakes triggered by poroelastic  
26 deformations at hypocentral depths. The catalog is produced by a best-fit water level curve  
27 ~~superimposed on the~~and by regional strike-slip tectonic deformations. The earthquakes of this  
28 synthetic catalog show an ~~impressing~~impressive agreement with historicalal earthquakes  
29 documented to damage Jerusalem. We demonstrate for the first time a high correlation between  
30 water level changes and the recorded recurrence intervals of historicalal earthquakes.

## 31 **KEYWORDS**

32 Seismic recurrence interval; Water level changes; Effective stress; Dead Sea

## 33 **INTRODUCTION**

34 ~~Triggering of e~~Earthquakes induced by water level changes in lakes and reservoirs has been  
35 a focus of seismic investigations around the world (e.g. Simpson et al., 1988; Pandey and Chadha,  
36 2003; Durá-Gómez and Talwani, 2010). Triggering is attributed to a drop in the effective normal  
37 stress at a fault, induced by water level change at the overlying lake's bed (Simpson et al., 1988;  
38 Durá-Gómez and Talwani, 2010; Hua et al., 2013b; Gupta, 2018). This kind of triggering may be  
39 particularly significant for areas with moderate and low tectonic strain accumulations (Pandey and  
40 Chadha, 2003; Gupta, 2018), such as the Dead Sea fault in the Middle East (e.g., Masson et al.,  
41 2015).

42 Seismic activity due to water level change was observed beneath artificial reservoirs  
43 immediately after their first filling (e.g., Simpson et al., 1988; Hua et al., 2013 a). It also appeared

44 after several seasonal filling cycles (Simpson et al., 1988; Talwani, 1997), explained by diffusion  
45 of pore pressure to the earthquake's hypocentral depth via the fault (Durá-Gómez and Talwani,  
46 2010). In addition, reservoir-induced seismicity sometimes manifests itself at long distances away  
47 from the reservoir (e.g., at 35 km, Durá-Gómez and Talwani, 2010). The correspondence of this  
48 kind of contemporary seismicity to water level change is usually identified based upon real-time  
49 data.

50 Alternatively, on a much longer time scale, changing seismic activity may also be associated  
51 with water level changes in historical al water bodies (e.g., the Dead Sea, since 2 ka, Fig. 1A, in the  
52 Appendix, which occupies the tectonic depression along the Dead Sea fault). Water level hikes of  
53 ~15 m, characteristic for time intervals of centuries to millennia, were analyzed in Belferman et  
54 al., (2018) and shown to be able to moderate the seismicity pattern at the Dead Sea fault  
55 ~~(Belferman et al., 2018).~~

56 However, reconstruction of fluctuations in historical al lake levels and the concurrent  
57 seismicity are both subject to significant uncertainties. They stem from the differing nature of the  
58 data gathered on these two phenomena, and thus deserve special consideration. Earthquake dating  
59 can be quite precise, and its accuracy is verified when different historical sources show consensus  
60 (Guidoboni et al., 1994; Guidoboni and Comastri, 2005; Ambraseys, 2009). Assessment of the  
61 extent of damage (hence earthquake magnitude), similarly requires such a consensus between the  
62 different data sources. Sediment records can help to calibrate the analysis of the historical evidence  
63 (Agnon, 2014; Kagan et al., 2011). Such records can be tested by trenching (Wechsler et al., 2014;  
64 Marco and Klinger, 2014; Lefevre, 2018). However, in many cases earthquake epicenter can be

65 imprecise or not even known. Consequently, considerable uncertainty pertains to the historical  
66 catalog of earthquakes related directly to the Dead Sea.

67 By contrast, historical water level records are quite precise elevation wise, as they are  
68 obtained from different points around the lake (Bookman et al., 2004; Migowski et al., 2006).  
69 However, water level dating could have an error of about  $\pm 45$  yr, as estimated from the  
70 radiocarbon dating of shoreline deposits in fan delta outcrops (Bookman et al., 2004). This may  
71 underestimate the actual dating uncertainty due to reworking of organic matter, sometimes re-  
72 deposited a century or more after equilibration with the atmosphere (Migowski et al., 2004). In  
73 addition, the entire past bi-millennial Dead Sea level record is constrained by less than twenty  
74 “anchor points” (the data obtained by the dating collected from surveyed paleo-shorelines,  
75 Bookman et al., 2004). Therefore, its continuous reconstruction, as suggested in the literature  
76 (Migowski et al., 2006; Stern, 2010), usually takes different forms within the acceptable limits  
77 dictated by the evidence, geomorphological (Bookman et al., 2004) and limnological-evidence,  
78 (Migowski et al., 2006; Bookman et al., 2004). A challenging uncertainty for our study arises from  
79 the interpolations required for periods when the available data ~~does~~ not constrain the water levels.

80 In this article, we take advantage of the correlation between the historical water level  
81 reconstructions at the Dead Sea and seismicity patterns in the area over the past two millennia. We  
82 demonstrate for the first time that plausible scenarios for the lake level history can fit very well the  
83 record of the historical earthquake recurrence intervals (RIs). Based on the correlation between  
84 these phenomena, we offer an alternative explanation regarding the triggering of ~~the~~ earthquakes  
85 in the area of the Dead Sea.

## 86 METHODS

87 To investigate the ~~relation~~relationship between an accurate but discrete chronology of  
88 earthquakes and the continuous water level (WL) change, we first explore the space of possible  
89 WL histories by a statistical approach. We generate an ensemble of WL curves (based on the  
90 anchor points ~~(~~Bookman et al., 2004), while remaining within the limits dictated by climatic and  
91 morphological constraints (Bookman et al., 2004; Migowski et al., 2006 ~~and~~; Stern, 2010), by  
92 using a random number generator.

93 In our analysis we associate all the historical earthquakes presented (Table 1A,2A in  
94 Appendix) with rupture of the strike-slip faults, which agree with our modeling approach. Hence,  
95 the major strike-slip faults constituting the plate boundary (Lower Jordan fault, Dead Sea Lake  
96 fault and Northern Arava) could be affected by Dead Sea water level changes. Therefore, our study  
97 covers the area within this distance.

98

99 A best fit random method of WL curve prediction

100 The compilation of WL curves of the Dead Sea for the last two millennia from three recent  
101 publications (Bookman et al., 2004; Migowski et al., 2006 and Stern 2010) is presented in Figure  
102 1A by dashed curves. Generally, the differences between all dashed curves at anchor points is  
103 included within an error limit of  $\pm 45$  yr as indicated by error bars, with an exception of the anchor  
104 point dated to 1400 CE (Bookman et al., 2004) for which Migowski et al. (2006) and Stern (2010)  
105 suggested a higher WL. Nevertheless, each hypothetical WL curve is forced to pass through all  
106 anchor points ~~provided by~~according to Bookman et al. (2004) except for one, at around 500 CE.  
107 The WL drop around this time, according to Migowski et al. (2006) and Stern (2010), occurred

108 later than was originally suggested by Bookman et al. (2004) (Figure 1A). Because this shift is  
109 within the permissible error limits ( $\pm 45$  yr), this anchor point is shifted to the left (+40 yr). In  
110 addition, the WL determined on the curve edges of the studied bi-millennial time interval was  
111 defined by additional two anchor points, through which the estimated WL curve passed according  
112 to all three references. In total, we have 13 anchor points. Between each pair of points, the trends  
113 in the WLs are constrained by the sedimentary facies (Migowski et al., 2006) that specify the edge  
114 points of the interval as the extrema for the acceptable WL variation.

115 However, within the largest interval between the anchor points (600 - 1100 CE), the field  
116 studies (Migowski et al., 2006; Stern, 2010; Bookman et al., 2004) constrained the WL to be lower  
117 than the extrema at the edges of that interval. For this period, the WL was randomly interpolated  
118 between the higher (e.g., Migowski et al., 2006) and lower (e.g., Stern, 2010) bounds. To maintain  
119 a monotony of the WL variation (required by the facies analysis of Migowski et al.), a moving  
120 average filtered the random noise between every pair of the anchor points. Accounting for the  
121 above-mentioned limits, and setting a ten-year step, the model has generated 10 million WL curves  
122 for the last ~~bi-millennial~~bimillennial interval, using a uniformly distributed random number  
123 generator.

124 We test for linear correlation between the recurrence intervals (RIs) of the widely recorded  
125 moderate-to-large ( $M > 5.5$ ) historical earthquakes available from the literature (~~see~~ Table 1 and  
126 the text description in Appendix), and the ~~generated~~ WL interpolations. ~~The test is given~~ (as in  
127 Figure 9 in Belferman et al., 2018) ~~by~~; and evaluate the ~~value~~values of the Pearson product-  
128 moment correlation coefficient, R (Figure 1B). We use this statistic for evaluating the suitability  
129 of each randomly interpolated WL curve for our analysis, for identification and elimination of  
130 any outliers, and for studying the behavior of the entire ensemble of the curves generated.

## 131 The earthquake simulation algorithm

132 The most suitable WL curve suggested by this correlation (discussed in the results section  
133 below), was used to generate a “synthetic” earthquake catalog based on the algorithm described  
134 in this section. Effective (normal) poroelastic stress change due to the WL change is  
135 superimposed on the tectonic stress accumulated consistently with the slip rate since the  
136 preceding seismic event, and synthetic earthquakes are simulated using a Coulomb failure  
137 envelope and a Mohr circle (e.g. Jaeger et al., 2009). A vertical ~~outplane~~ strike-slip fault below  
138 the lake/reservoir bed is assumed (simulating a Dead Sea fault), embedded in the 2D (plain  
139 strain) geometry of the upper crust (~~see~~ Belferman et al., 2018). Tectonic horizontal strike-slip  
140 displacements ~~at~~ across the fault are approximated by a simple shear approach with no normal  
141 strain component.

142 In the poroelastic part of the model, horizontal stress change normal to the strike slip fault  
143 produced by the water level change, is calculated under a uniaxial (vertical) strain condition  
144 (Eq.10b in Belferman et al., 2018). This is applicable to a post-diffusion stage: i.e., when pore  
145 pressure at hypocentral depth ~~equilibrates with~~ ~~approaches that at~~ the lake’s bed. An array of the  
146 effective horizontal normal stress changes,  $\Delta\sigma'_i$ , at the fault, induced by the water load change at  
147 the lake’s bed,  $p_{s_i}$ , corresponds to the array of the WL change,  $\Delta h_i$  ( $i = 1, 2, \dots, 2000$ ) over the  
148 interpolated water level curve, Figure 1D:

149 1. 
$$\Delta\sigma'_i = \frac{1-2\nu}{1-\nu} (\beta - 1) p_{s_i}$$

150 (~~see~~ Eq. 10b in Belferman et al., 2018). Here  $\beta$  is Biot's coefficient and  $\nu$  is the Poisson's ratio,  
151  $p_{s_i} = \rho g \Delta h_i$ , where  $\rho$  is the density of water and  $g$  is the acceleration of gravity.

152 A radius and a centre location of the Mohr circle change as a function of the tectonic  
153 deformations and water level changes, correspondingly, eventually reaching a failure envelope that  
154 simulates an earthquake. The model uses a Byerlee's law envelope (Byerlee, 1978) to define the  
155 residual strength of a seismogenic zone at the fault immediately after the earthquake (see  
156 Belferman et al., 2018 for more detail). Since the effective stress upon the onset of an earthquake  
157 is specified by a high failure envelope and the effective stress following the slip is given by the  
158 Byerlee's law (e.g., Belferman et al., 2018;), the model is time-predictable. The stress drop, at least  
159 in the nucleation zone of a single-fault model, is expected to be proportional to the recurrence  
160 interval.

161 The starting point of the simulations is the date of the first historical earthquake (33CE,  
162 see Table 1 in the Appendix) from the bi-millennial time interval studied. The simulation  
163 incrementally proceeds with time over the WL curve generated (as above) under the accumulating  
164 tectonic stress. After each stress release, the time to the next earthquake,  $\Delta t$ , is calculated from the  
165 solution of the Mohr-Coulomb failure criterion for a strike-slip tectonic regime and a WL change,  
166  $\Delta h_i$ , applicable to  $\Delta h_i$ , characteristic of the Dead Sea fault (Belferman, et al., 2018):

$$2. \quad (\tau_i - \tau_0)^2 + (\sigma_i - (\sigma_0 + \Delta\sigma'_i))^2 = (R_0 + \Delta\tau_{xy_i})^2$$

$$168 \quad \tau_i = C + \tan(\varphi)\sigma_i$$

169 assuming that  $\Delta\tau_{xy_i} = \frac{C \cos(\varphi)}{t_{RI}} \Delta t$  is the tectonic shear stress accumulated consistently with  
170 slip rate at the strike-slip fault during the period  $\Delta t$  (time passed since the last earthquake),  
171  $C$  is cohesion,  $\varphi$  is an angle of internal friction,  $\sigma_0$  and  $\tau_0$  are the coordinates of the Mohr circle



172 center immediately after the earthquake and  $R_0$  its radius,  $t_{RI}$  is the reference RI corresponding to  
173 the minimal WL.

174 For each time step, the algorithm determines whether there is a single solution, or two, or  
175 nil. A case of no solutions means that the Mohr circle is yet to reach the failure envelope, as the  
176 accumulating tectonic stress and the WL increase are still insufficient. The system of Eq. 2 may  
177 have a single solution when the failure criterion is met~~earthquake occurs~~ at the end of some  
178 timestep, or two solutions when ~~the failure criterion~~ is met before the end of the timestep. A case  
179 of two solutions is rounded down to a case of a single solution if a time step (one year) is small  
180 compared to the earthquake RI (several hundreds of years).

181 This solution of Eq.2 yields a RI as a function of the effective normal horizontal stress  
182 change,  $\Delta\sigma'_i$  (Belferman et al., 2018):

$$183 \quad 3. \quad RI = \Delta t = (C + \tan(\varphi)\Delta\sigma'_i) \frac{t_{RI}}{C}$$

184 where  $t_{RI}$  is the reference ~~RI corresponds~~ RI corresponding to the minimal WL,  $C$  is cohesion,  $\varphi$   
185 is an angle of internal friction. From this formula~~for RI~~, an array of earthquake dates is obtained.

186 ~~Substituting~~ Substitution of Eq.1 into Eq.3, ~~we get~~ yields a linear dependence of a simulated RI  
187 ason a ~~linear function of~~ WL change,  $\Delta h_i$ , evolving with time~~;~~.

$$188 \quad 4. \quad RI = t_{RI} + \frac{\tan(\varphi)}{C} \frac{1-2\nu}{1-\nu} (\beta - 1) \rho g t_{RI} \Delta h_i$$

189 A tectonic slip-rate is set at 5 mm/yr (e.g. Hamiel et al., 2018; Hamiel and Piatibratova, 2019;  
190 Masson et al., 2015). Coefficients for the simulations were previously determined in Belferman et  
191 al. (2018). Note that the cohesion,  $C$ , is not a-priory known, hence it is fixed by the empirical  
192 correlation between WL and RI for a given lake level history considered. ~~In addition, the Its slip-~~

193 ~~rate is set at 5 mm/yr (e.g. Hamiel et al., 2018; Hamiel and Piatibratova, 2019; Masson et al., 2015).~~  
194 ~~The change in WL is calculated relative to its minimal level (415 m bmsl) over the period. A~~  
195 ~~cohesion~~ value,  $C = 0.08\text{Mpa}$ , and a reference RI,  $t_{RI} = 300\text{yr}$ , were adjusted numerically for a  
196 ~~specific~~ WL curve, providing the average RI of 144 yr over the ~~modelled~~modeled period of two  
197 millennia justified by historical, archaeological, and geological data (Agnon, 2014).

## 198 **RESULTS**

199 Ten most suitable WL curves(~~Figure 2~~) are identified out of the 10M set of WL randomly  
200 generated curves (“ensemble”) by the Pearson product-moment correlation test. The values of the  
201 correlation coefficients, R, for the entire ensemble are distributed normally around  $R=0.63$  (Figure  
202 1B) with a standard deviation of  $\sigma =0.076$ . The ten most suitable WL curves ordered by their  
203 correlation coefficients, R, are presented in Figure 2.

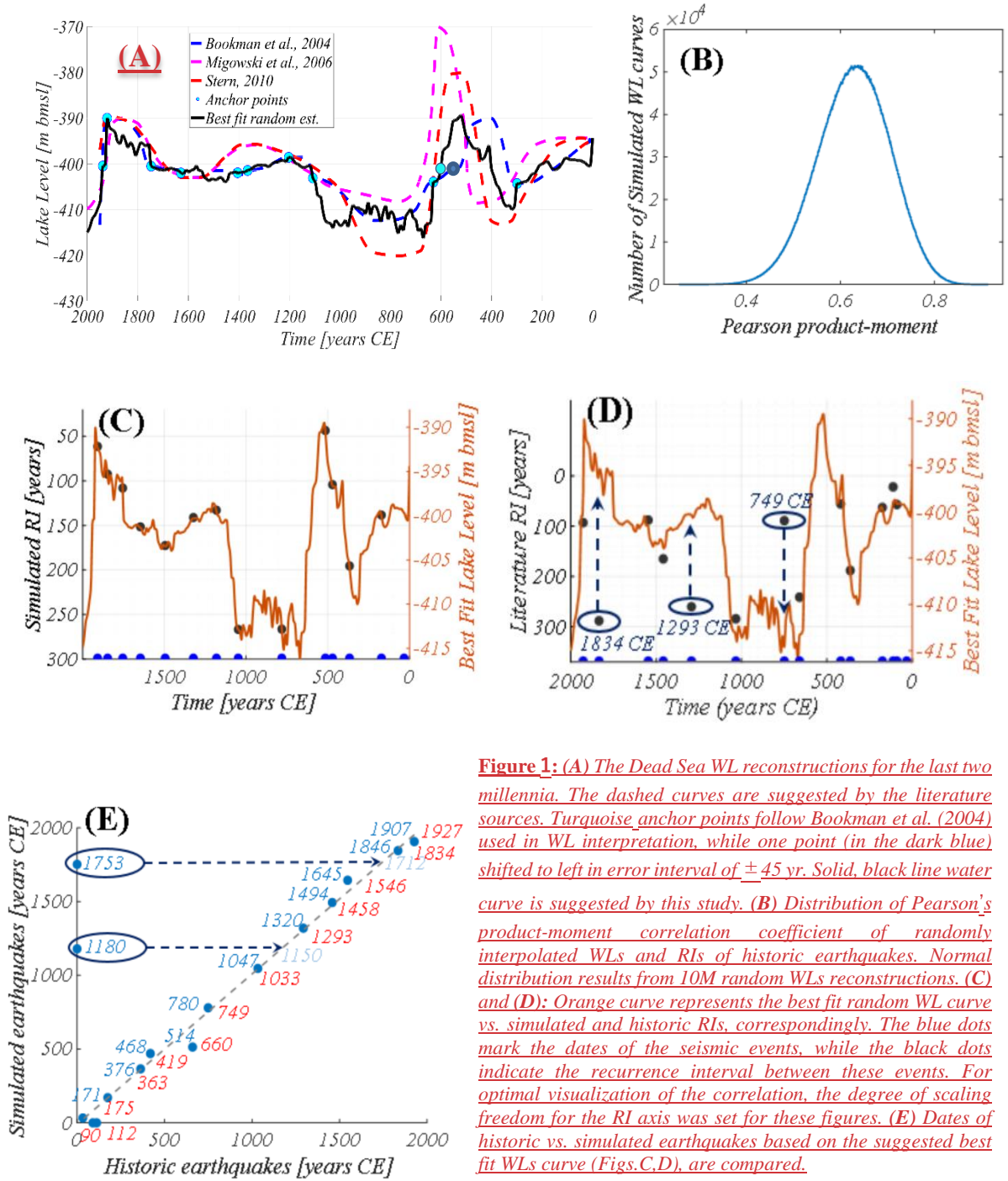


**Figure 1:** (A) The Dead Sea WL reconstructions for the last two millennia. The dashed curves are suggested by the literature sources. Turquoise anchor points follow Bookman et al. (2004) used in WL interpretation, while one point (in the dark blue) shifted to left in error interval of  $\pm 45$  yr. Solid, black line water curve is suggested by this study. (B) Distribution of Pearson's product-moment correlation coefficient of randomly interpolated WLs and RIs of historic earthquakes. Normal distribution results from 10M random WLs reconstructions. (C) and (D): Orange curve represents the best fit random WL curve vs. simulated and historic RIs, correspondingly. The blue dots mark the dates of the seismic events, while the black dots indicate the recurrence interval between these events. For optimal visualization of the correlation, the degree of scaling freedom for the RI axis was set for these figures. (E) Dates of historic vs. simulated earthquakes based on the suggested best fit WLs curve (Figs.C,D), are compared.



**Figure 2:** Ten most suitable WLs identified out of the 10M randomly generated by the Pearson product-moment correlation test.

206 Three outliers from the thirteen RIs of the widely recorded historic earthquakes (749 CE,  
207 1293 CE, and 1834 CE in Figure 1) were identified and reevaluated (~~see the~~ explanation in  
208 Appendix). A curve with athe highest Pearson coefficient of R=0.912 was chosen from the  
209 correlation between the RIs of the revised historic catalog and the randomly generated WLs:  
210 (Figure 2). This correlation can be specified by a linear prediction function:

211 5.  $RI = -5442 - 14WL$

212 where RI is given in years and WL in meters. In addition, a synthetic earthquake history including  
213 14 seismic events was simulated from the best fit randomly interpolated WL curve with R=1  
214 specified above. The ~~correlation between the~~ synthetic RIs can be approximated based on the and  
215 WLs using the linear relationship Eq.4 (presented in Figure 1C) is:

216 6.  $RI = -3840 - 10WL$

217 ~~as expected from the linear dependence suggested by the analytical solution (Eq.4)~~. The dates of  
218 the simulated synthetic earthquakes are presented, versus the dates of the historical al earthquakes  
219 from the literature (Table A1, Appendix) in Figure 1E.

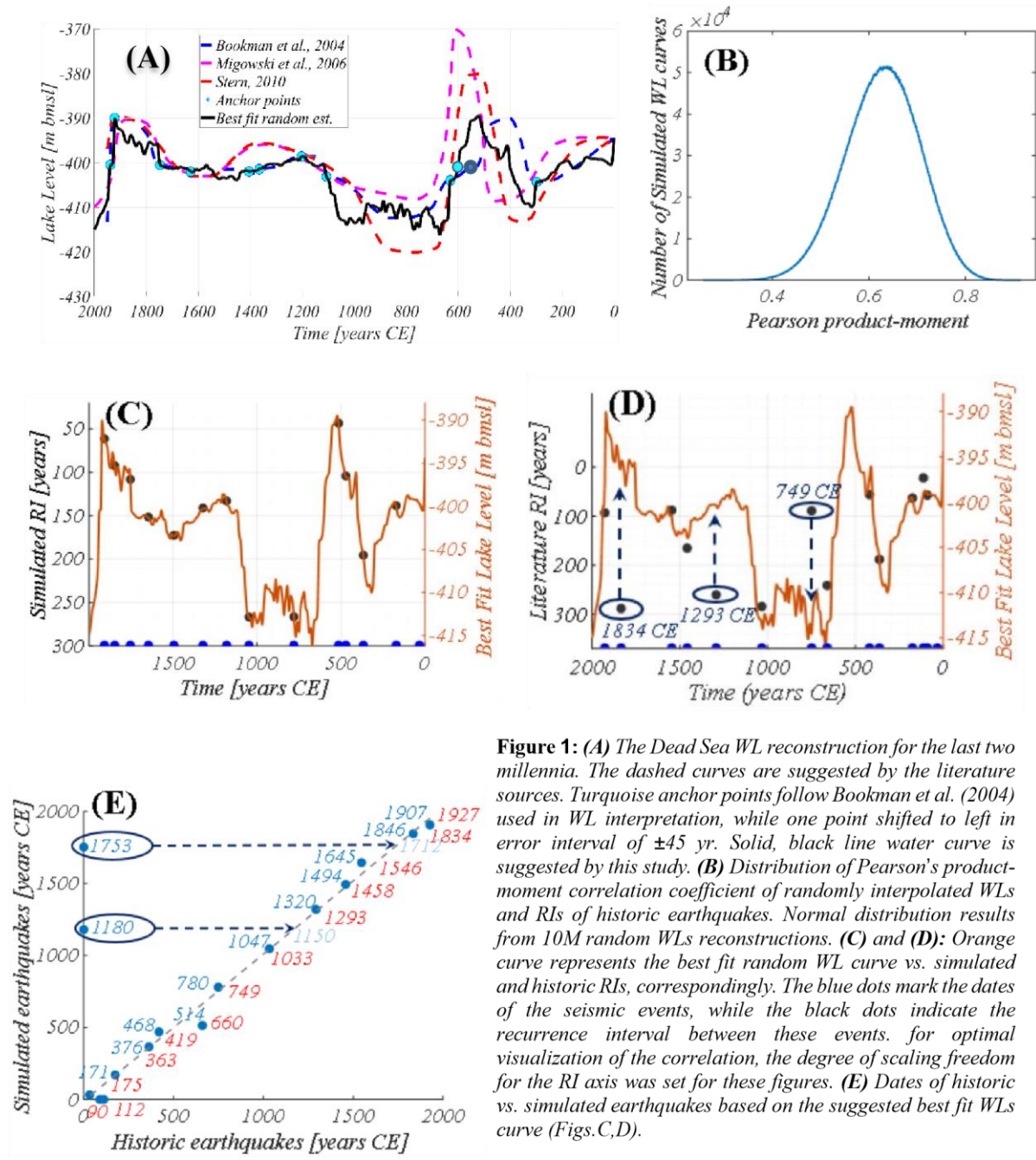


**Figure 1:** (A) The Dead Sea WL reconstruction for the last two millennia. The dashed curves are suggested by the literature sources. Turquoise anchor points follow Bookman et al. (2004) used in WL interpretation, while one point shifted to left in error interval of  $\pm 45$  yr. Solid, black line water curve is suggested by this study. (B) Distribution of Pearson's product-moment correlation coefficient of randomly interpolated WLs and RIs of historic earthquakes. Normal distribution results from 10M random WLs reconstructions. (C) and (D): Orange curve represents the best fit random WL curve vs. simulated and historic RIs, correspondingly. The blue dots mark the dates of the seismic events, while the black dots indicate the recurrence interval between these events. For optimal visualization of the correlation, the degree of scaling freedom for the RI axis was set for these figures. (E) Dates of historic vs. simulated earthquakes based on the suggested best fit WLs curve (Figs. C,D).



203 **Figure 2:** Ten-most suitable WLs identified out of the 10M randomly generated by the Pearson product moment

1        The synthetic earthquake stress history is presented in Figure 3. The effective horizontal  
2        normal stress change,  $\Delta\sigma'_i$ , (Figure 3A) linearly depends on the water level (Eq.1.), and as  
3        expected, follows its variability. The tectonic shear stress change,  $\Delta\tau_{xy}$ , drops to zero after the  
4        accumulated shear stress is released by the strike-slip earthquake (Figure 3B). Less shear stress is  
5        required to induce the earthquake when the change in water level is larger (Figures 3A,3B),  
6        modeled with Mohr-Coulomb failure criteria (Figure 3C) (explained also in Belferman et. al.,  
7        2018).



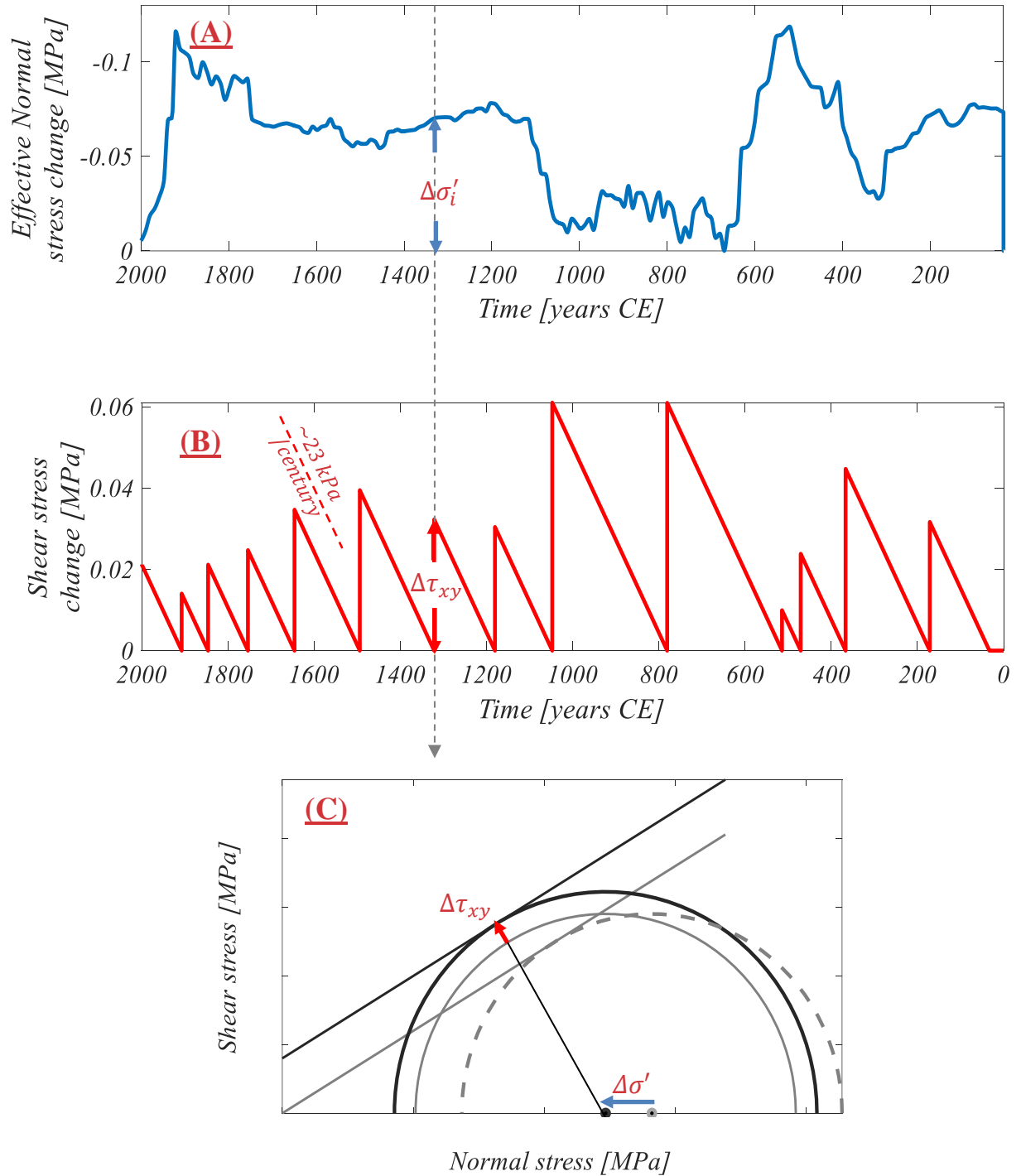


**Figure 3:** (A) The effective normal stress change,  $\Delta\sigma'$ , induced by water level change, Eq.1. (B) Tectonic shear stress change,  $\Delta\tau_{xy}$ , accumulated consistently with slip-rate on the strike-slip fault during the time passed since the last earthquake. The shear stress accumulation rate, used in this study is about 23 kPa/century (formulation below Eq. 2, following Belferman et al., 2018) (C) Evolution of the stress change on the fault due to combined tectonic and water loading. The state of the effective stress at the fault immediately after an earthquake is restricted by the Byerlee's law envelope with zero cohesion,  $C=0$ , and a friction angle,  $\varphi = 0.54^\circ$ . The center of the Mohr circle is located at  $(\sigma_0, \tau_0=0)$  see Belferman et al., 2018 for more detail). The failure envelope is defined by  $C>0$  and  $\varphi = 0.54^\circ$ . The left shift in the center of the circle by  $\Delta\sigma'$  represents pore pressure (due to water level) change at this moment (Fig.3A); the increase in radius represents tectonic shear stress,  $\Delta\tau_{xy}$ , accumulated during the inter-seismic period (Fig.3B). Failure occurs when the circle tangents the failure envelope (presented here for the representative 1320 CE earthquake).

## 9 DISCUSSION

10       Uncertainties in the WL reconstructions associated with dating and resolution lead to  
11 considerable variance in possible interpolations (Figure 1B). A Pearson correlation coefficient test  
12 shows that most of the randomly interpolated WL curves give linear correlation with earthquake  
13 RIs (indicated by a mean Pearson coefficient of  $R=0.63$ ), excluding the three outliers (Figure 1D)  
14 to be discussed below. Figure 2 shows a similar pattern of the WL change for the ten most  
15 correlated curves. In all cases, a significant rise in the water level of about 400 CE and 1100 CE is  
16 visible and a decrease in the WL around 200 and 600 CE. Also, the maximum level around 500  
17 and 1900 CE appears in all ten cases.

18       For simulating synthetic earthquakes triggered by the WL change, we use the WL curve that  
19 generates the highest correlation with the revised historical catalog ( $R = 0.912$ ) (Figure 2). The  
20 dates of these simulated synthetic earthquakes are comparable with historical earthquakes (Figure  
21 1E) excluding two events, whose date labels are offset to the y-axis for clarity of presentation  
22 (1753 CE, 1180 CE). The dates of these synthetic earthquakes might be connected to three outliers  
23 from the historical catalog (1834 CE, 1293 CE, and 749 CE depicted in Figure 1D) as explained  
24 below.

25       The 1180 CE synthetic earthquake (Figure 1E) is comparable to an earthquake in the  
26 literature dated by Ben-Menachem (1979) and Amiran et al. (1994) to the mid-12th century (~1150  
27 CE). Ambraseys (2009) doubted the precise dating but accepted this mid-12th century estimate.  
28 The damaged area of this earthquake spanned Jericho and Jerusalem, and the event could be  
29 considered ~~as~~ significant, because it led to the total destruction of two monasteries, one of which  
30 is 10 km south of Jerusalem's curtain wall. By admitting the ~1150 CE earthquake to the amended

31 catalog, we reduce the RI of the subsequent earthquake at 1293 CE (Figure 1D) from 260 to 143  
32 yrs, thereby bringing this outlier very close to the linear correlation.

33 Our model also generates an earthquake in the 18th century, dated 1753 CE, for which there  
34 were no matches in our initial historical catalog (Belferman et al., 2018). However, in Amiran's et  
35 al. (1994) catalog an earthquake in 1712 CE is indicated: 'The quake shook the solid houses and  
36 ruined three Turkish houses. Felt in Ramle, but not in Jaffa'. Additionally, this earthquake is  
37 evidenced by seismites dated to 1700 – 1712 CE from an Ein Gedi site (Migowski et al., 2004).

38 Regarding the modeled 1907 CE event, we note the well-documented (although often  
39 overlooked) 29 March 1903 CE earthquake (Amiran et al., 1994). This was a moderate but  
40 prolonged earthquake: local intensity reached VII in a number of localities distributed outside the  
41 rift valley over an area of 140x70 square km (including Jerusalem), whereas the maximum  
42 intensity reported in the rift was VII as well (Jericho). We prefer to correlate the modeled 1907  
43 event with the stronger 1927 Jericho earthquake that clearly released stress in the Dead Sea (e.g.  
44 Shapira, et al., 1993; Avni et al., 2002; Agnon, 2014). This leaves the 1903 CE unmatched to our  
45 model. Perhaps the earthquake ruptured the northern part of the central Jordan Valley, north of the  
46 Dead Sea and south of Lake Kinneret (Sea of Galilee).

47 Regarding the last outlier from the historical earthquakes dated to 749 CE (or its neighbors  
48 747 and 757, Table A1 in the Appendix) (Figure 1D) and corresponding to the simulated 780 CE  
49 earthquake (Figure 1E): the simulation generated the preceding earthquake 514 CE associated with  
50 the 659/660 CE event from the literature (Table A1 in the Appendix) with a deviation of 146 years.  
51 The rupture zone of the 659/660 CE event is uncertain, and this earthquake is not necessarily  
52 related to stress-release at the Dead Sea basin. Alternatively, following Russell (1985), as a result

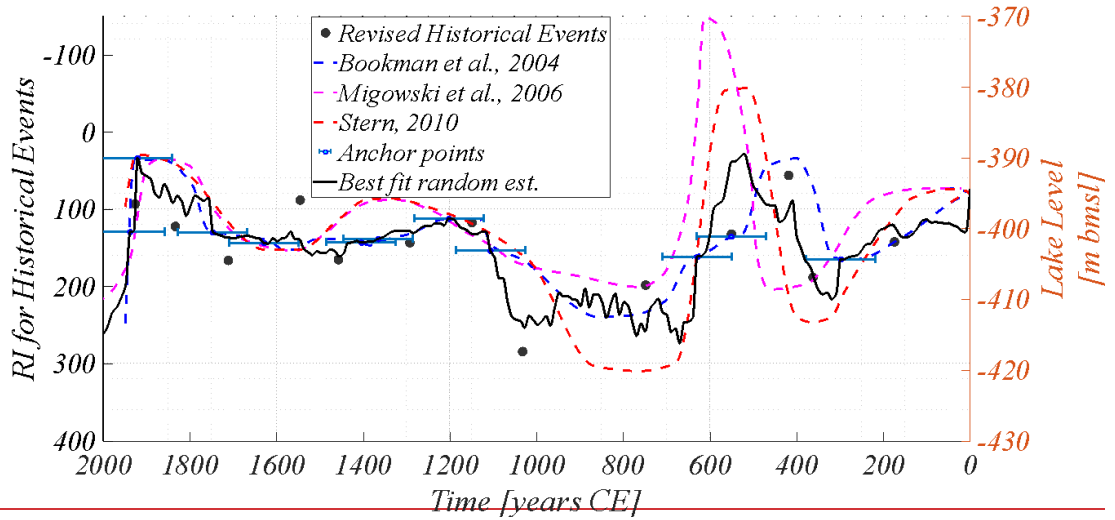
53 of the 551 CE earthquake, a fortress east of the southern Dead Sea and Petra were destroyed.  
54 Newer data contradicts the assertion regarding Petra; a failure ~~at~~in the Dead Sea region is still  
55 plausible. Replacing the 660 CE earthquake with 551 CE in the catalog changes the RI preceding  
56 the 749 CE historical earthquake from 89 to 198, which brings this outlier into a satisfactory linear  
57 correlation (Figure 1D).

58 Additionally, it should be emphasized that in the simulation presented in this article, the  
59 starting point is quite arbitrarily, the earthquake of ~~33CE~~33 CE. This event together with the  
60 subsequent earthquakes ~~90CE~~90 CE and ~~112CE~~112 CE (not predicted by our model) span a single  
61 century where the catalog is nebulous. Each of these events could thus represent the starting point  
62 of the simulations or could be omitted at this early and poorly documented interval.

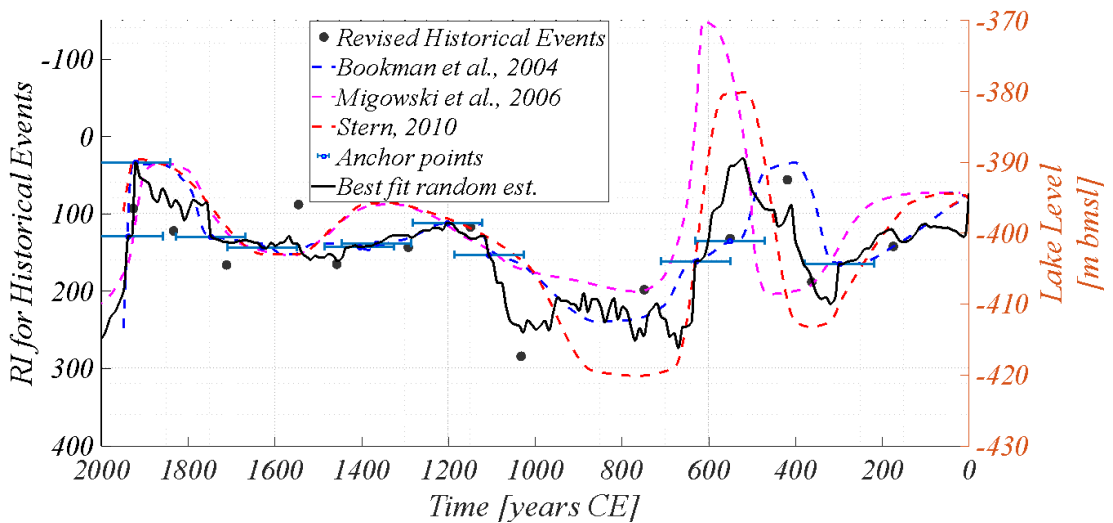
63 Summarizing the above amendments, we add to our catalog of historicalal events the 551 CE,  
64 ~1150 CE, and 1712 CE, earthquakes, and remove 559/660 CE and ~~90CE~~90 CE, 112 CE  
65 earthquakes (Figure 1E). Altogether, we get 14 triggered historicalal earthquakes.

66 The correlation between the water level and recurrence interval is noticeable for the various  
67 variants of the water level curve reconstruction (Figure ~~3~~-4).

68



69



70 **Figure 34:** The Dead Sea WL reconstruction for the last two millennia. The dashed curves are suggested by the literature. Blue  
 71 anchor points with an error interval of  $\pm 45$  yr. follow Bookman et al. (2004). The solid black line is the water level curve suggested  
 72 by this study. The black points represent the RI for revised historical events, suggested in this study as being relevant to the Dead  
 73 Sea area.

74 The correlation of RI with the best fit random estimated curve can be specified by a linear  
 75 prediction function:

76 7.  $RI = -2483 - 6.5WL$

77 This linear relationship between WL and RI underscores the previously proposed  
78 correlations between these phenomena (in Figure 9 in Belferman et al., 2018).

79 Since the last earthquake (~~1927~~1927 CE), the water level in the Dead Sea has  
80 continuously decreased at an average annual rate of ~1 m/yr. Today the water level is about -440  
81 (m bmsl), thus our prediction function (Eq. 7) suggests an RI of 377 yr, for such a WL.  
82 ~~Namely~~Alternatively, should~~if~~ the water level in the Dead Sea ~~should~~ remain constant (-440 m  
83 bmsl), as intended in some mitigation plans, we would expect the next earthquake at about ~2300  
84 ~~yr~~CE.

85 This paper stresses that reconstructions of WL curves ~~are~~is not unique and may take various  
86 forms under the constraints available (e.g., Figure 1A). However, the correlation with an  
87 independent record of RIs of seismic events, assuming that earthquakes are affected by WL hikes,  
88 allows deciphering plausible scenarios for WL evolution. Moreover, for cases with the best but  
89 not perfect correlation, the deviation might be consistent with a release of elastic energy by smaller  
90 earthquakes, which are not accounted for by the deterministic part of our model. We note that  
91 smaller earthquakes might rupture dip-slip fault planes, again not accounted for by our simple  
92 model.

93 Additionally, as large earthquakes are accompanied by aftershocks, some of the elastic  
94 energy is released by them. ~~Moreover, it was shown earlier, in areas where earthquakes caused by~~  
95 ~~artificial reservoirs, how this mechanism influenced by water level change.~~ It was shown earlier  
96 that in areas of reservoir-induced seismicity, earthquakes are not only accompanied by aftershocks  
97 but also preceded by foreshocks (Gupta, 2011). The decay curve of this kind of seismicity satisfies  
98 the criteria for the second class of earthquake sequences by Mogi (1963). The lack of instrumental

99 records of historical earthquakes in our study area, does not allow comparison with this class. The  
100 1995 Gulf of Aqaba earthquake (7.2 Mw), the last large instrumentally recorded earthquake, was  
101 accompanied by a long period (significant enough for stress release consideration) of the  
102 aftershocks. The earthquake occurred along the southern part of the plate boundary, which is far  
103 enough from the Dead Sea, and most likely is not influenced by the water level change. Following  
104 this earthquake, felt aftershocks continued for about two years. At least 50 percent of the total  
105 moment associated with these aftershocks was released during the first day after the main shock  
106 and over 95 percent in the first 3 months (Baer, 2008). In total, the post-seismic moment released  
107 during the period of 6 months to 2 yr after the Nuweiba earthquake is about 15 percent of the co-  
108 seismic moment release (Baer, 2008). This earthquake showed that the response of the crust to  
109 earthquakes by aftershocks is negligible, as noted for many large earthquakes (e.g., Scholz, 1972).

110 For the case of artificial reservoirs, it was shown that for reservoir-induced seismicity  
111 sequences, aftershocks continue for a longer time than for tectonic earthquake sequences (Gupta,  
112 2011). However, because given the time scale of RI, the period of aftershocks is insufficient to  
113 consider earthquakes from the sequence in our model as separate events. Regarding the time scale  
114 presented in our study, when the minimal inter-seismic period is about 50 years, the stress released  
115 during a post seismic period can be considered a part of the main shock.

116 The mechanical model used in this article is rather simplistic, where earthquakes release the  
117 strike-slip component of the tectonic loading- (Figure 3B). The basins around the Dead Sea fault  
118 system also testify for ~~also~~ an extensional component that could be manifested in co-seismic  
119 motion along normal faults. To justify our focus on a single type of fault (strike-slip), we list the  
120 following arguments:

- 121 • The far-field maximal and minimal principal stresses in the Dead Sea region are horizontal  
122 (Hofstetter et al., 2007; Palano et al. 2013). This is compatible with ~~athe~~ dominance of  
123 ~~strikeslip~~strike-slip faulting (Anderson, 1951). The tectonic motion at the DSF is  
124 characterized predominantly by a left-lateral strike-slip regime with a velocity of ~5 mm/yr  
125 along various segments (Garfunkel, 2014; Masson et al.,2015; Sadeh et al., 2012). Large  
126 earthquakes that initiate clusters are likely to rupture along the straight ~100 km strike-slip  
127 segments (Lyakhovsky et al., 2001). The strike of these segments parallels the relative plate  
128 velocity vector and thus can be approximated by ~~a~~ simple shear. Additionally, in the Dead  
129 Sea basin, GPS surveys indicate the dominance of ~~strike~~strike-slip loading. Hamiel et al.  
130 (2018) show that, on a plate scale, horizontal shear loading dominates the velocity north of  
131 the lake. Hamiel and Piatibratova (2019) detected a sub-mm/yr component of extension  
132 across the southern normal fault bounding the Dead Sea ~~pull-pull-apart,~~ (Amatzyahu  
133 Fault); yet the strike-slip component across this very fault ~~seems-is~~ much larger.
- 134 • Normal, as well as strike-slip faults, similarly react to water level change that contributes  
135 to the vertical stress component and pore pressure change. The seismicity induced by  
136 surface water level fluctuations and affected by the faulting regime is critically determined  
137 by the relative orientations of the three principal stresses in the Earth's crust (Anderson,  
138 1951). In regions where the vertical compressive stress is not minimal (normal and strike-  
139 slip faulting), seismic activity is more sensitive to the effective stress change due to water  
140 level change, than in regions where it is minimal (thrust faulting) (Simpson, 1976; Snow,  
141 1982; Roeloffs, 1988). This is applicable to ~~a case of~~ reservoirs approximated as “infinite”  
142 in the horizontal plane (e.g., Wang, 2000), with respect to the fault zone horizontal cross-  
143 section. Since we are using a one-dimensional model, such approximation is valid for our



144 study area where the Dead Sea is large enough in a horizontal plane (100 km x 10 km)  
145 compared to the thickness of the underlying strike-slip fault (cross-section) located in the  
146 central part of the valley.

147 Our results demonstrate that a fairly simple forward model (based on 1D analytical  
148 solution, Belferman et al., 2018) achieves a ~~very good~~convincing correlation between WLs and  
149 RIs of moderate-to-strong earthquakes on the Dead Sea fault. Whereas the fault system along the  
150 Dead Sea fault is more complicated, three-dimensional modeling of the tectonic motion, coupled  
151 ~~to~~with the pore pressure evolution, may give more reliable predictions regarding earthquake  
152 ruptures and their chronology. However, based on the relationship between the WL and RI changes  
153 presented in this article, with the current anthropogenic decrease in the Dead Sea level (with an  
154 average annual rate of ~ 1 m / yr), a moderate to severe earthquake will not be triggered by the  
155 mechanism discussed here. This article not only ~~presents~~suggests the existence of a connection  
156 between WL and RI, but also provides additional guidance based on this connection, ~~also about~~  
157 ~~the uncertainties regarding the two phenomena separately.~~

## 158 DATA AVAILABILITY

159 All raw data can be provided by the corresponding authors upon request.

## 160 AUTHOR CONTRIBUTIONS

161 MB and AA Conceptualization; AA data collection and analysis; MB Modelling, data  
162 visualization and results analysis; RK Validation; MB original draft preparation; MB, RK and AA  
163 review and revisions; AA, ZB and RK Funding acquisition and Resources.

## 164 COMPETING INTERESTS

165 The authors declare that they have no conflict of interest.

166 **ACKNOWLEDGMENTS**

167 This project was supported by ~~the~~ grants from the Ministry of Natural Infrastructures,  
168 Energy and Water Resources of Israel # 213-17-002, ~~and~~ GIF- German - Israeli Foundation for  
169 Scientific Research and Development # I-1280-301.8., and by PhD fellowships from the  
170 University of Haifa, Israel. The data for this paper ~~was~~were obtained with analytical and numerical  
171 modeling.

172 **REFERENCE**

- 173 Agnon A. 2014. Pre-instrumental earthquakes along the Dead Sea rift. In Dead Sea transform fault  
174 system: reviews, edited by Garfunkel, Zvi, Ben-Avraham, Zvi, Kagan, Elisa, 207-261,  
175 Springer, Dordrecht. [https://doi.org/10.1007/978-94-017-8872-4\\_8](https://doi.org/10.1007/978-94-017-8872-4_8).
- 176 Ambraseys, N. 2009. Earthquakes in the Mediterranean and Middle East: a multidisciplinary study  
177 of seismicity up to 1900. Cambridge University Press. doi:  
178 <https://doi.org/10.1017/CBO9781139195430>
- 179 Ambraseys, N. N., Melville, C. P. and Adams, R. D. 1994. The Seismicity of Egypt, Arabia and  
180 the Red Se: A Historical Review. Cambridge: Cambridge Univ. Press.  
181 <https://doi.org/10.1017/S1356186300007240>
- 182 Amiran, D. H., ArieH, E., and Turcotte, T. 1994. Earthquakes in Israel and adjacent areas:  
183 macroscopic observations since 100 B.C.E. Israel Exploration Journal, 44, 260– 305.  
184 <http://www.jstor.org/stable/27926357>.
- 185 Anderson, E. M. (1951). The dynamics of faulting and dyke formation with applications to Britain.  
186 Oliver and Boyd. Avni, R., Bowman, D., Shapira, A. and Nur, A. 2002. Erroneous  
187 interpretation of historical documents related to the epicenter of the 1927 Jericho

188 earthquake in the Holy Land. *Journal of seismology*, 6(4), 469-476.  
189 <https://doi.org/10.1023/A:1021191824396>

190 Baer G., G. J. Funning, G. Shamir, T. J. Wright (2008). The 1995 November 22, Mw 7.2 Gulf of  
191 Elat earthquake cycle revisited, *Geophysical Journal International*, 175(3), 1040-  
192 1054. <https://doi.org/10.1111/j.1365-246X.2008.03901.x>

193 Belferman, M., Katsman, R. and Agnon, A. 2018. Effect of large-scale surface water level  
194 fluctuations on earthquake recurrence interval under strike-slip faulting. *Tectonophysics*,  
195 744, 390-402. <https://doi.org/10.1016/j.tecto.2018.06.004>

196 Ben-Menahem, A. 1979. Earthquake catalogue for the Middle East (92 BC-1980 AD). *Boll.*  
197 *Geofis. Teor. Appl.*, 21, 245-313.

198 Bookman, R., Enzel, Y., Agnon, A., and Stein, M. 2004. Late Holocene lake levels of the Dead  
199 Sea. *Geological Society of America Bulletin* 116, 555-571. <https://doi.org/10.1130/B25286.1>

200 Byerlee, J.D., 1978. Friction of rocks. In: Byerlee, J.D., Wyss, M. (Eds.), *Rock Friction and*  
201 *Earthquake Prediction. Springer, Birkhäuser, Basel*, pp. 615–626.  
202 <https://doi.org/10.1007/978-3-0348-7182-2>

203 Durá-Gómez, I. and Talwani, P. 2010. Reservoir-induced seismicity associated with the Itoiz  
204 Reservoir, Spain: a case study, *Geophysical Journal International*, 181, 343–356.  
205 <https://doi.org/10.1111/j.1365-246X.2009.04462.x>

206 Elad, A. 1982. An early [arabieArabic](#) source concerning the markets of Jerusalem. *Cathedra*, 24,  
207 31-40.

208 Elad, A., 1992. Two Identical Inscriptions From Jund Filastin From the Reign of the Abbāsīd  
209 Caliph, Al-Muqtadir. *Journal of the Economic and Social History of the Orient*, 35(4),  
210 301-360. <https://doi.org/10.2307/3632739>

211 Garfunkel, Z., 2014. Lateral motion and deformation along the Dead Sea Transform. In: Garfunkel,  
212 Z., Ben-Avraham, Z., Kagan, E. (Eds.), *Dead Sea Transform Fault System: Reviews*. 5.  
213 Springer, Dordrecht, pp. 109–150. <http://dx.doi.org/10.1007/978-94-017-8872-4>.

214 Gerber, H., 1998. " Palestine" and Other Territorial Concepts in the 17th Century. *International*  
215 *Journal of Middle East Studies*, 30(4), 563-572. <https://www.jstor.org/stable/164341>

216 Guidoboni, E., Comastri, A., and Traina, G. 1994. *Catalogue of Ancient Earthquakes in the*  
217 *Mediterranean Area Up to the 10th Century*. Rome: Istituto nazionale di geofisica.  
218 <https://doi.org/10.1163/182539185X01377>

219 Guidoboni, E. and Comastri, A. 2005. *Catalogue of Earthquakes and Tsunamis in the*  
220 *Mediterranean Area from the 11th to the 15th Century*. Istituto nazionale di geofisica e  
221 vulcanologia. <https://doi.org/10.1515/BYZS.2008.854>

222 Gupta, H., K., 2018, Reservoir triggered seismicity (RTS) at Koyna, India, over the past 50  
223 yrs. *Bulletin of the Seismological Society of America* 108.5B: 2907-2918.  
224 <https://doi.org/10.1785/0120180019>

225 Hamiel, Y., Masson, F., Piatibratova, O., & Mizrahi, Y. (2018). GPS measurements of crustal  
226 deformation across the southern Arava Valley section of the Dead Sea Fault and  
227 implications to regional seismic hazard assessment. *Tectonophysics*, 724, 171-178.  
228 <https://doi.org/10.1016/j.tecto.2018.01.016>

229 Hamiel, Y., & Piatibratova, O. (2019). Style and distribution of slip at the margin of a pull-apart  
230 structure: Geodetic investigation of the Southern Dead Sea Basin. *Journal of Geophysical*  
231 *Research: Solid Earth*, 124(11), 12023-12033. <https://doi.org/10.1029/2019JB018456>

232 Hofstetter, R., Klinger, Y., Amrat, A. Q., Rivera, L., & Dorbath, L. (2007). Stress tensor and focal  
233 mechanisms along the Dead Sea fault and related structural elements based on  
234 seismological data. *Tectonophysics*, 429(3-4), 165-181.  
235 <https://doi.org/10.1016/j.tecto.2006.03.010>

236 Hua, W., Chen, Z. and Zheng, S., 2013a. Source parameters and scaling relations for reservoir  
237 induced seismicity in the Longtan reservoir area. *Pure Appl. Geophys.* 170, 767–783.  
238 <https://doi.org/10.1007/s00024-012-0459-7>

239 Hua, W., Chen, Z., Zheng, S., and Yan, C., 2013b. Reservoir-induced seismicity in the Longtan  
240 reservoir, southwestern China. *J. Seismol.* 17 (2), 667–681.  
241 <https://doi.org/10.1007/s10950-012-9345-0>

242 Hough S. E. and Avni R., 2011. The 1170 and 1202 CE Dead Sea Rift earthquakes and long-term  
243 magnitude distribution of the Dead Sea Fault Zone, *Isr. J. Earth Sci.*, 58, 295–308.  
244 <https://doi.org/10.1560/IJES.58.3-4.295>

245 Jaeger, J. C., Cook, N. G., & Zimmerman, R. (2009). *Fundamentals of rock mechanics*. John Wiley  
246 and Sons.

247 Kagan, E., Stein, M., Agnon, A., and Neumann, F. 2011. Intrabasin paleoearthquake and  
248 quiescence correlation of the late Holocene Dead Sea. *Journal of Geophysical Research:*  
249 *Solid Earth*, 116(B4). <https://doi.org/10.1029/2010JB007452>

250 Ken-Tor, R., Agnon, A., Enzel, Y., Stein, M., Marco, S., and Negendank, J. F. 2001. High-  
251 resolution geological record of historic earthquakes in the Dead Sea basin. *Journal of*  
252 *Geophysical Research-Solid Earth*, 106, 2221-2234.  
253 **<https://doi.org/10.1029/2000JB900313>**

254 Langgut, D., Yannai, E., Taxel, I., Agnon, A. and Marco, S., 2015. Resolving a historical  
255 earthquake date at Tel Yavneh (central Israel) using pollen seasonality. *Palynology*, 40(2),  
256 145-159. **<https://doi.org/10.1080/01916122.2015.1035405>**

257 Lefevre, M., Klinger, Y., Al-Qaryouti, M., Le Béon, M. and Moumani, K., 2018. Slip deficit and  
258 temporal clustering along the Dead Sea fault from paleoseismological investigations. *Sci.*  
259 *Rep.* 8 (1), 4511. **<https://doi.org/10.1038/s41598-018-22627-9>**

260 Lyakhovskiy, V., Ben-Zion, Y., Agnon, A., 2001. Earthquake cycle, fault zones, and seismicity  
261 patterns in a rheologically layered lithosphere. *J. Geophys. Res. Solid Earth* 106 (B3),  
262 4103–4120.

263 Marco, S., Stein, M., Agnon, A., and Ron, H. 1996. Long-term earthquake clustering: A 50,000-  
264 year paleoseismic record in the Dead Sea Graben. *Journal of Geophysical Research: Solid*  
265 *Earth*, 101(B3), 6179-6191. **<https://doi.org/10.1029/95JB01587>**

266 Masson, F., Hamiel, Y., Agnon, A., Klinger, Y. and Deprez, A., 2015. Variable behavior of the  
267 Dead Sea Fault along the southern Arava segment from GPS measurements. *comptes*  
268 *rendus geoscience*, 347(4), pp.161-169. **<https://doi.org/10.1016/j.crte.2014.11.001>**

269 Migowski, C., Agnon, A., Bookman, R., Negendank, J. F., and Stein, M. 2004. Recurrence pattern  
270 of Holocene earthquakes along the Dead Sea transform revealed by varve-counting and

271 radiocarbon dating of lacustrine sediments. *Earth and Planetary Science Letters*, 222, 301–  
272 314. <https://doi.org/10.1016/j.epsl.2004.02.015>

273 Migowski, C., Stein, M., Prasad, S., Negendank, J. F. W., and Agnon, A. 2006. Holocene climate  
274 variability and cultural evolution in the Near East from the Dead Sea sedimentary record.  
275 *Quaternary Research*, 66(3), 421-431. <https://doi.org/10.1016/j.yqres.2006.06.010>

276 Palano, M., Imprescia, P., & Gresta, S. (2013). Current stress and strain-rate fields across the Dead  
277 Sea Fault System: Constraints from seismological data and GPS observations. *Earth and*  
278 *Planetary Science Letters*, 369, 305-316. <https://doi.org/10.1016/j.epsl.2013.03.043>

279 Pandey, A.P. and Chadha, R.K., 2003. Surface loading and triggered earthquakes in the Koyna–  
280 Warna region, western India. *Phys. Earth Planet. Inter.* 139 (3–4), 207–223.  
281 <http://dx.doi.org/10.1016/j.pepi.2003.08.003>

282 Parker, S.T., 1982. Preliminary Report on the 1980 Season of the Central " Limes Arabicus"  
283 Project. *Bulletin of the American Schools of Oriental Research*, 247(1), pp.1-26.  
284 <https://www.journals.uchicago.edu/doi/10.2307/1356476>

285 Rao, N. P., & Shashidhar, D. (2016). Periodic variation of stress field in the Koyna–Warna  
286 reservoir triggered seismic zone inferred from focal mechanism  
287 studies. *Tectonophysics*, 679, 29-40. <https://doi.org/10.1016/j.tecto.2016.04.036>

288 Russell, K. W., 1985. The earthquake chronology of Palestine and northwest Arabia from the 2nd  
289 through the mid-8th century AD. *Bulletin of the American Schools of Oriental*  
290 *Research*, 260(1), 37-59. <https://doi.org/10.2307/1356863>

291 Sadeh, M., Hamiel, Y., Ziv, A., Bock, Y., Fang, P., Wdowinski, S., 2012. Crustal deformation  
292 along the Dead Sea Transform and the Carmel Fault inferred from 12 years of GPS  
293 measurements. *J. Geophys. Res. Solid Earth* 117, B08410.  
294 <http://dx.doi.org/10.1029/2012JB009241>.

295 Scholz, C. H. (1972). Crustal movements in tectonic areas. *Tectonophysics*, 14(3-4), 201-217.  
296 [https://doi.org/10.1016/0040-1951\(72\)90069-8](https://doi.org/10.1016/0040-1951(72)90069-8)

297 Shapira, A., Avni, R., and Nur, A. 1993. A new estimate for the epicenter of the Jericho earthquake  
298 of 11 July 1927. *Isr. J. Earth Sci*, 42(2), 93-96.

299 Simpson, D. W. (1976). Seismicity changes associated with reservoir loading. *Engineering*  
300 *Geology*, 10(2-4), 123-150. [https://doi.org/10.1016/0013-7952\(76\)90016-8](https://doi.org/10.1016/0013-7952(76)90016-8)

301 Simpson, D. W., Leith, W., and Scholz, C. 1988. Two types of reservoir-induced seismicity.  
302 *Bulletin of the Seismological Society of America*, 78, 2025–2040.

303 Snow, D. T. (1982). Hydrogeology of induced seismicity and tectonism: Case histories of Kariba  
304 and Koyna. *Geological Society of America Special Papers*, 189, 317-360.  
305 <https://doi.org/10.1130/SPE189-p317>

306 Stern, O. 2010. Geochemistry, Hydrology and Paleo-Hydrology of Ein Qedem Spring System;  
307 Report GSI/17/2010; Geological Survey of Israel: Jerusalem, Israel, 2010; p. 91. (In  
308 Hebrew)

309 Talwani, P., 1997. On the nature of reservoir-induced seismicity. *Pure Appl. Geophys.* 150, 473–  
310 492. [https://doi.org/10.1007/978-3-0348-8814-1\\_8](https://doi.org/10.1007/978-3-0348-8814-1_8)



311 Wang, H., 2000. Theory of Linear Poroelasticity With Applications to Geomechanics and  
312 Hydrogeology. University Press, Princeton.

313 Wechsler, N., Rockwell, T. K., Klinger, Y., Štěpančíková, P., Kanari, M., Marco, S., & Agnon, A.  
314 (2014). A paleoseismic record of earthquakes for the Dead Sea transform fault between the  
315 first and seventh centuries CE: Nonperiodic behavior of a plate boundary fault. *Bulletin of*  
316 *the Seismological Society of America*, 104(3), 1329-1347. <https://doi.org/10.1785/0120130304>

317 Williams, J. B., Schwab, M. J., & Brauer, A. 2012. An early first-century earthquake in the Dead  
318 Sea. *International Geology Review*, 54(10), 1219-1228.  
319 <https://doi.org/10.1080/00206814.2011.639996>

## 320 **Appendix: The earthquake history of the Dead Sea environs**

321 Numerous publications list earthquakes that hit the Dead Sea and its surroundings during the last  
322 two millennia (e.g. Agnon, 2014; Ambraseys et al., 1994; Ambraseys, 2009; Amiran et al., 1994;  
323 Guidoboni et al., 1994, Guidoboni and Comastri, 2005). In Belferman et al. (2018) we adopted  
324 from the scores of listed events only the most destructive ones, typically causing local intensities  
325 of VII or higher in Jerusalem. For a minimal epicentral distance of 30 km, this would translate to  
326 a magnitude of ~5.7 or higher (according to the attenuation relation of Hough and Avni, 2011).

327 Table A1 lists the Dead Sea earthquakes considered for stress release across the Dead Sea basin  
328 during the last two millennia. We used two criteria: noticeable damage in fortified Jerusalem, and  
329 seismites in the northern Dead Sea. Our simple model simulates an earthquake time series, given  
330 a water level curve. Eleven events from this time series correlate with events of magnitude ~6 or  
331 more in the [historical](#) record. Yet, the model generates four events that are not included in our  
332 original catalog. On the other hand, a single event (~660 CE) listed in Belferman et al. (2018) has

333 no counterpart in the simulations despite a wide range of level curves tested. All these curves are  
334 generated by a random number generator, subject to constraints from field data. We first discuss  
335 the four events required by the simulations one by one. Then we review the ~660 CE event along  
336 with other historical events that were left out already in Belferman et al. (2018).

337 The earthquakes in Table 1 are classified according to the level of acceptance for being destructive  
338 in Jerusalem. The nine events of **Class C** are all consensual, also used by Belferman et al. (2018).  
339 These events appear in all catalogs and lists and need no further discussion. The six events of **Class**  
340 **A** are debated events, accepted in the present study. All earthquakes in this class are selected by  
341 simultaneously satisfying two criteria: (1) The acceptance regularizes the relation between  
342 recurrence intervals and lake level; (2) They are corroborated by evidence from seismites in the  
343 northern basin of the Dead Sea (Ein Feshkha and Ein Gedi sites, Fig.A1 corroborate).

344 We chose the year **33 CE** to start our simulations. While this earthquake did not cause a widespread  
345 damage, it was recorded in all three seismite sites (Kagan et al., 2011), with a maximum of decade  
346 uncertainty based on dating by counting lamina under the microscope (Migowski et al., 2004;  
347 Williams et al., 2012).

348 The second entry in Table A1, **~100 CE**, refers to two decades of unrest. Migowski et al. (2004)  
349 identified a pair of seismites around 90 CE and 112 CE in the 'Ein Gedi Core. The corresponding  
350 sequences in Ein Feshkha and Ze'elim Creek are laminates, attesting to quiescence. A historical  
351 hiatus between the Roman demolition of Jerusalem and the erection of Ilya Capitolina in its stead  
352 (70-130 CE) preclude historical evidence. Although damage to the Masada fortress has been  
353 assigned to an earthquake **1712 CE**.

354 Table A2 lists ten earthquakes that have been reported to damage around Jerusalem but are not  
355 required by our simulations. The seven events of **Class R** are the debated events, rejected here

356 after discussion. The three **Class S** events were skipped altogether in that compilation of  
357 Ambraseys (2009).

358 Of the seven Class R events, the 7 June **659** CE earthquake was accepted by us in Belferman et al.  
359 (2018). The earthquake has been associated with destruction of the Euthymius monastery 10 km  
360 east of Jerusalem, but no damage in the town of Jerusalem has been unequivocally reported  
361 (Ambraseys, 2009). In Belferman et al. (2018) we included this event in the catalog of Dead Sea  
362 earthquakes, as Langgut et al. (2015) have located it on the center of the Jordan Valley segment of  
363 the transform (Figure A1). However, this interpretation neglected the possibility that the rupture  
364 could have been outside the hydrological effect of the Dead Sea basin. One of the lessons of our  
365 numerous simulations is that our model would not support triggering of this earthquake shortly  
366 (less than a century) before the mid-8th century crisis, when lake levels were dropping to the lowest  
367 point in the studied period (420 m bsl, Figure 1a). When rejecting the 659 CE event, the 419 CE  
368 earthquake is the one preceding the mid-8th century crisis; the three century recurrence interval  
369 fits well the low lake level.

370 **1016** CE: The collapse of the Dome of the Rock was not explicitly attributed to an earthquake by  
371 the original sources, who found it enigmatic as well (Ambraseys, 2009).

372 **1644** CE: Ambraseys (2009) quoted a late Arab author, al-Umari, who reported collapse of houses  
373 and deaths of five persons in “the town of Filistin”. While Ambraseys has interpreted it probably  
374 to Jerusalem, it might refer to al-Ramla, the historical capital of the classical Filistin District, as in  
375 “al-Ramla, Madinat Filastin” (Elad, 1992, p335). Or, it is a mistranslation of “Bilad Filistin” which  
376 at that time started refer to the entire Holy Land district, without specifying a town (Gerber, 1998).  
377 Jerusalem, at that time, was called Bayt el Maqdis or, as nowadays, al-Quds. The only report of an  
378 earthquake in Jerusalem around 1644 mentions horror but no structural damage - the 1643 CE

379 event that Ambraseys (2009) tends to equate with the 1644 CE event. A seismite in Ein Gedi core  
380 can be correlated with this event (Migowski et al., 2004, Table 2, entry 6). Migowski et al. (2004)  
381 have identified the seismite with the 1656 earthquake that was felt in Palestine; Ambraseys' (2009)  
382 interpretation was not yet available for them.

383 **1656 CE:** This event was strong in Tripoli and only felt in Palestine. Migowski et al. (2004)  
384 correlated it to a seismite based on deposition rates (no lamina counting for that interval). Given  
385 the 1644 CE entry of Ambraseys (2009), this interpretation should be revised, and the 1656 CE  
386 earthquake is not to be associated with any local rupture in the Dead Sea.

387 Table A1: A ~~catalog~~ *catalog* of earthquakes that could potentially damage Jerusalem. The classes  
 388 denote the level of acceptance of damage to Jerusalem among the researchers: C - consensual; B  
 389 - accepted by Belferman et al., 2018; A - amended here; R - rejected here.  
 390

Year CE or Century (marked C)	C l a s s	Seismite correl. by site			Reference	Comments
		Z E †	E G <sup>y</sup>	E F <sup>o</sup>		
33	B	+	+	+	MI,K&,W&	Identified in all three seismites sites, varve-counted to 31 BCE
100~	B	-	2	-	MI,AM	Seismites ~90 and ~112; questionable archaeological evidence
~175	B	-	+	-	MI	A seismite; no historical or archeological support
363	C	-	-	+	K&,A&	A seiche in the Dead Sea, a seismite at EF <sup>o</sup> (north Dead Sea)
419	C	+	+	+	KT/MI/K&	
551	A	+	+	+	PA,AM	
<b>747/9,757</b>	C	+	+	+	KT/MI/K&	
1033	C	?	+	+	KT/MI/K&	
~1150	A	+	-	/	AM,K&	I <sub>0</sub> IX - Mar Elias (& Qasr al-Yahud) monasteries demolished
1293	C	+	+	+	K&	
1458	C	+	+	h	MI	
1546	C	/	+	i	MI	
1712	A	/	+	a	MI	A& / I <sub>0</sub> VII - “ruined three Turkish houses in Jerusalem”
1834	C	+	+	t	KT,MI	
1903	R	m	m	u	A&,AM	I <sub>0</sub> VII Mt. of Olives; several shocks, I <sub>0</sub> up to VII over a large area
1927	C	+	+	s	KT,MI	AV / I <sub>0</sub> VII-VIII in and around Jerusalem (I <sub>0</sub> 7.8 by GMPE)

391  
 392  
 393  
 394

395  
396  
397  
398

**Table A2:** Events listed in some catalogs and subsequently skipped (Class S) or declined (Class D) by Ambraseys (2009), or rejected (Class R) in the present study.

Year CE	C l a s s	Seismite correl. by site			Reference	Comments
		Z E †	E G <sup>‡</sup>	E F °		
~659	R	-	+	+	L&,AM	Jordan Valley, possibly over 65 km NE of Jerusalem
808	S	/	-	?	A&	
1016	D	?	?	?	AM,A&	Damage to the Dome of Rock, no specific reference to shaking
1042	S	-	+	-	BM	Syria, off the Dead Sea transform
1060	S	/	-	+	A&,SB	The roof of Al-Aqsa collapsed
1063	R				A&,AM,SB	Syrian littoral
1068	D	+	+	+	AM	Neither of the two events can be associated with the Dead Sea
1105	D	?	?	?	A&,AM	“Strong” but “no damage recorded in the sources”
1114	D	+	+	?	A&,AM	1114 - no damage around the city, a swarm, Kingdom’s north
~1117	R	+		?	A&,AM	
1557	R				Am	Collapse in Jerusalem: a gun foundry, a forgery, an oven
1644	R	h	+*	h	Am	Some damage and death toll in Palestine, likely Seismite 6 of MI
1656	R	h	-	h	A&,AM,SB	Tripoli VII, Palestine IV, MI misidentified with Seismite 6
1817	R				AM	Two churches damaged in Jerusalem, Holy Sepulchre affected
1870	S	?	-	h	AM	Mediterranean source

399 Abbreviations and notes:

400 †ZE - Ze' elim Creek; ‡EG - Ein Gedi core; °EF - Ein-Feshkha Nature Reserve

401 AM: Ambraseys, 2009; A&: Amiran et al., 1994; K&: Kagan et al., 2011; L&: Langgut et al.

402 2015; KT: Ken-Tor et al., 2004; MI: Migowski et al., 2004; PA: Parker, 1982; W&: Williams et

403 al., 2012.

404

405

406

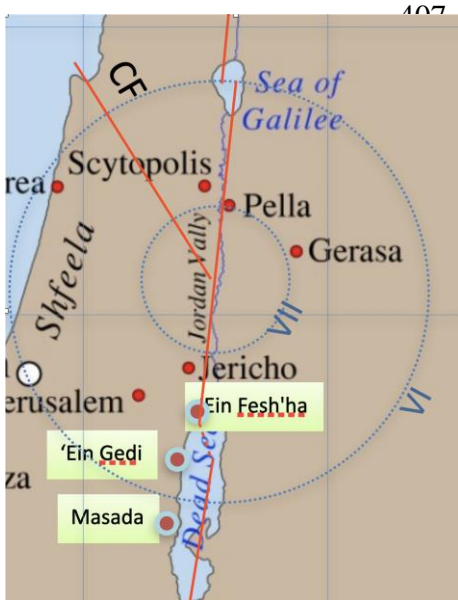


**Figure A1:** A map showing the epicenter reconstructed by Langgut et al. (2015) for the 659/660 CE mainshock.